

Time-Dependent Oxidative Degradation of WSe₂ Nanosheets and Its Influence on HER Catalysis

Panwad Chavalekvirat^{a,b}, Wisit Hirunpinyopas^c, and Pawin Iamprasertkun^{a,b,}*

^aSchool of Bio-Chemical Engineering and Technology, Sirindhorn International Institute of Technology, Thammasat University, Pathum Thani 12120, Thailand (pawin@siit.tu.ac.th).

^bResearch Unit in Sustainable Electrochemical Intelligent, Thammasat University, Pathum Thani 12120, Thailand.

^cDepartment of Chemistry, Faculty of Science, Kasetsart University, Bangkok 10900, Thailand

*Corresponding author: Pawin Iamprasertkun (pawin@siit.tu.ac.th)

<https://orcid.org/0000-0001-8950-3330>

This version is a preprint uploaded to arXiv and has not been peer-reviewed.

ABSTRACT

The selection of an appropriate solvent has long been a critical factor in the liquid phase exfoliation (LPE) of two-dimensional transition metal dichalcogenide (2D TMD) nanosheets. N-methyl-2-pyrrolidone (NMP) remains one of the most commonly used solvents due to its favourable surface tension compatibility, particularly with tungsten diselenide (WSe_2), which facilitates a relatively high yield of exfoliated nanosheets. However, prolonged exposure of the nanosheets to NMP promotes oxidation, consequently diminishing their hydrogen evolution reaction (HER) activity. In contrast, a more environmentally friendly solvent system, consisting of isopropyl alcohol (IPA) and deionised water (DI), induces significantly less oxidation and results in enhanced HER performance. Notably, this green solvent system achieves the lowest overpotential of 0.209 V vs RHE after 24 hours of chronoamperometry.

KEYWORDS: Liquid Phase Exfoliation, Solvent Selection, WSe_2 , Electrocatalysts, HER

INTRODUCTION

Transition metal dichalcogenides (TMDs) are promising alternatives to platinum-based catalysts for the hydrogen evolution reaction (HER)^{1, 2}. Among them, tungsten diselenide (WSe₂) has a suitable band gap, strong photoluminescence, and mechanical strength, contributing to its relatively high HER activity³⁻⁶. Notably, its electrochemical performance improves significantly after electrochemical cycling⁷, with the 2D form showing much higher HER activity than its bulk counterpart⁸. Therefore, synthesising 2D WSe₂ nanosheets is essential, and solvent-assisted liquid-phase exfoliation (LPE) provides a simple, cost-effective method for their production⁹. Several LPE parameters affect both exfoliation efficiency and nanosheet quality. One study employed cascade centrifugation and found that WSe₂ nanosheets with smaller dimensions have superior HER activity¹⁰. Exfoliation power also affects the nanosheets' structure and HER performance. Our previous study found that lower power yields WSe₂ nanosheets with less oxidation and higher crystallinity, enhancing HER activity¹¹. However, oxide content remained around 50% due to the use of NMP, which promotes WSe₂ oxidation to WO₃, emphasising the importance of solvent selection in optimising nanosheets quality and performance. In this study, we propose the synthesis of WSe₂ nanosheets using IPA/DI as a greener alternative to NMP, based on the hypothesis that this solvent mixture induces less oxidation. We also hypothesise that oxidation progresses over time. To evaluate this, we investigate the time-dependent oxidation of WSe₂ in both solvent systems over durations ranging from one day to one year.

RESULTS & DISCUSSIONS

The detailed synthesis and characterisation procedures are described in the electronic supplementary information (ESI). As shown in the XRD patterns in [Figure 1a](#), only the WSe₂ nanosheets exfoliated in NMP and stored for one year exhibited characteristic peaks of hexagonal WO₃ at around 23.6° and 29.8°. Meanwhile, all samples displayed the characteristic peak of 2H-WSe₂ at around 13.6°, consistent with previously reported values^{12, 13}. While XRD provides structural information on WSe₂ nanosheets in the solid state, it does not capture local structure changes in dispersion. Therefore, liquid-phase XAS was conducted for a more detailed analysis. The XANES spectra for all WSe₂ samples are presented in [Figure S1](#) and [Table S1](#). As shown in [Figure 1b](#), the Fourier transform curves of EXAFS spectra reveal a first-shell W–O peak at approximately 1.5 Å and a W–Se peak near 2.1 Å across all samples. The W–Se peak progressively shifts to higher radial distances and becomes broader with increased time in the solvent, particularly in samples exfoliated in NMP. Meanwhile, the W–O peaks become more pronounced over time, dominating in NMP-exfoliated samples as early as one month; by one year, the W–Se peak is barely distinguishable. In contrast, IPA/DI-exfoliated samples show a relatively balanced presence of W–O and W–Se peaks up to one month, with the W–O peak only becoming dominant after one year (for further details, see [Figure S2](#) and [Table S2](#)). These findings indicate time- and solvent-dependent oxidation, especially in NMP, leading to oxidation-induced degradation characterised by increased structural disorder (amorphisation) and the formation of selenium vacancies in the exfoliated WSe₂ nanosheets. These results are consistent with previous studies^{11, 14}. Notably, as XAS was conducted in dispersion, the prominent W–O peaks may partly result

from solvent-derived oxygen interacting with the WSe₂ nanosheets. The XAS analysis of the solid-state samples is presented in Figure S3.

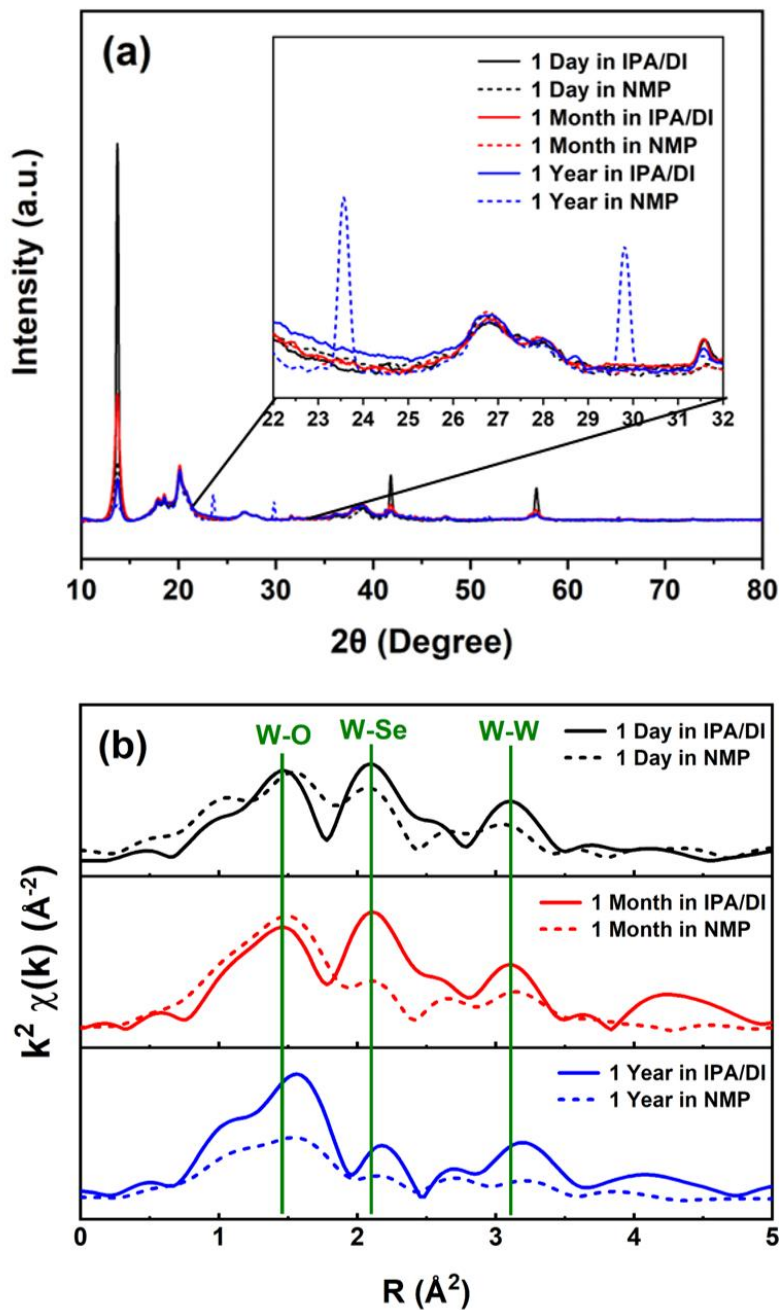


Figure 1. (a) X-ray diffraction patterns and (b) radial distances profiles EXAFS spectra of as-exfoliated WSe₂ samples in IPA/DI and NMP, for durations ranging from 1 day to 1 year.

To complement the analysis of the local structure, XPS was utilised to investigate the surface chemical composition of the exfoliated WSe₂ nanosheets. [Figure 2a](#) displays the W 4f XPS spectra for all exfoliated samples, revealing four distinct peaks: the W 4f_{7/2} and W 4f_{5/2} peaks of the W–Se bond at approximately 32.3 eV and 34.4 eV, as well as the W 4f_{7/2} and W 4f_{5/2} peaks of the W–O bond at around 35.8 eV and 37.9 eV, consistent with previous reports¹⁵. The IPA/DI-exfoliated samples exhibit more prominent W–Se peaks compared to those exfoliated in NMP. Over time, the W–O peaks become increasingly pronounced, ultimately dominating the spectra after one year of storage. This trend aligns with the XAS results, confirming the time- and solvent-dependent oxidation behaviour. As shown in [Figure 2b](#), the atomic concentrations of WSe₂ and WO₃ were quantified. The content of WO₃ is consistently higher in NMP-exfoliated samples and increases with storage duration. The IPA/DI-exfoliated sample stored for one day retains the highest WSe₂ concentration (~80%), while the NMP-exfoliated sample stored for one year shows a significant decrease to approximately 20%. This accelerated oxidation is attributed to the auto-oxidation of NMP in the presence of oxygen and moisture¹⁶. This reaction lowers the pH of the medium and facilitates the dissolution of transition metals, leading to the release of free tungsten atoms into the solvent¹⁷. These free W atoms are then exposed to dissolved oxygen, triggering oxide formation. Moreover, the reactive species produced during NMP auto-oxidation can directly oxidise the WSe₂ nanosheets, further promoting the generation of oxide species^{16, 18}. Additional XPS data for the Se 3d region and a detailed W 4f peak analysis are included in [Figure S4](#) and [Table S3](#).

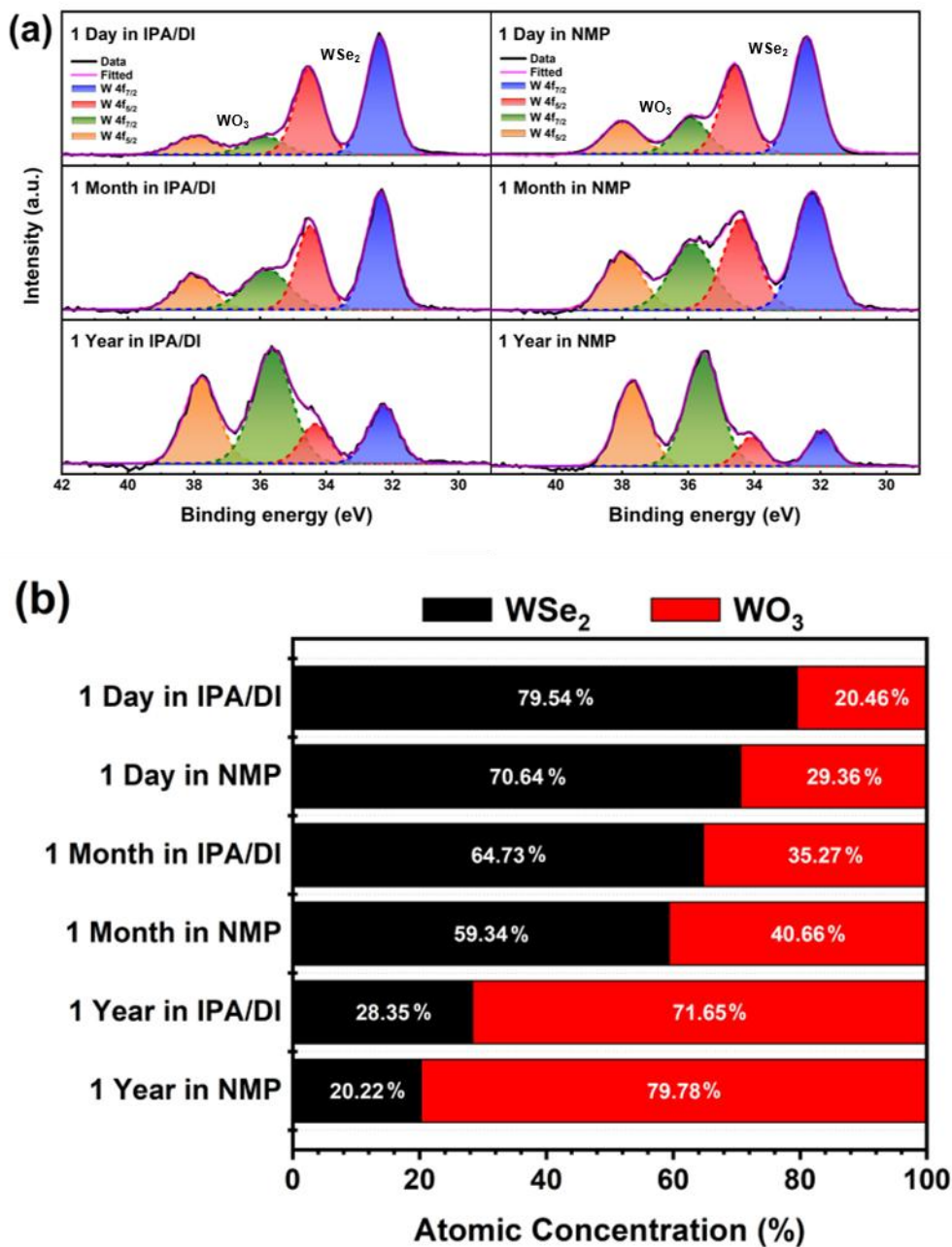


Figure 2. XPS analysis of the surface chemical composition of WSe₂ nanosheets exfoliated in IPA/DI and NMP over storage durations from 1 day to 1 year: (a) W 4f spectra and (b) atomic concentration ratios of WSe₂ to WO₃ for each sample.

While X-ray-based techniques have confirmed the time- and solvent-dependent oxidation of exfoliated WSe₂ nanosheets, their surface morphology and structural evolution required further investigation. To address this, TEM analysis was conducted, and the HR-TEM images of all WSe₂ samples are presented in Figure 3, with corresponding selected area electron diffraction (SAED) patterns shown in the insets. At a magnification of 500,000x, WSe₂ nanosheets exfoliated in IPA/DI (Figure 3a-c) retain clear crystallinity and exhibit the characteristic hexagonal lattice of 2H-WSe₂ across all storage durations. In contrast, for NMP-exfoliated samples, only the sample stored for one day (Figure 3d) maintains a visible hexagonal structure. By one month (Figure 3e), the lattice structure becomes indistinct, though the interplanar d-spacing can still be identified. After one year (Figure 3f), the lattice planes are no longer resolvable, suggesting significant structural degradation. This degradation is attributed to increased oxidation over time, especially in NMP, which promotes auto-oxidation of WSe₂ nanosheets. Interestingly, the relationship between oxide content and surface structure appears complex. Although the IPA/DI sample stored for one year exhibits a higher oxide content (~72%) than the NMP-exfoliated sample stored for one month (~40%), the latter shows a more significant structural loss, with the hexagonal framework no longer observable. This suggests that the NMP not only promotes oxidation but may also enhance the formation of selenium vacancies, accelerating amorphisation. These observations are further supported by SAED analysis. The insets of Figure 3a-d show distinct, bright dotted rings, characteristic of crystalline materials¹⁹. In the inset of Figure 3e (NMP, one month), the diffraction rings appear more diffuse and continuous. By one year (inset of Figure 3f), the rings become completely diffuse and thicker, indicating a transition to an amorphous structure¹⁹. This finding aligns well with the XAS results, further confirming the progressive structural disorder over time.

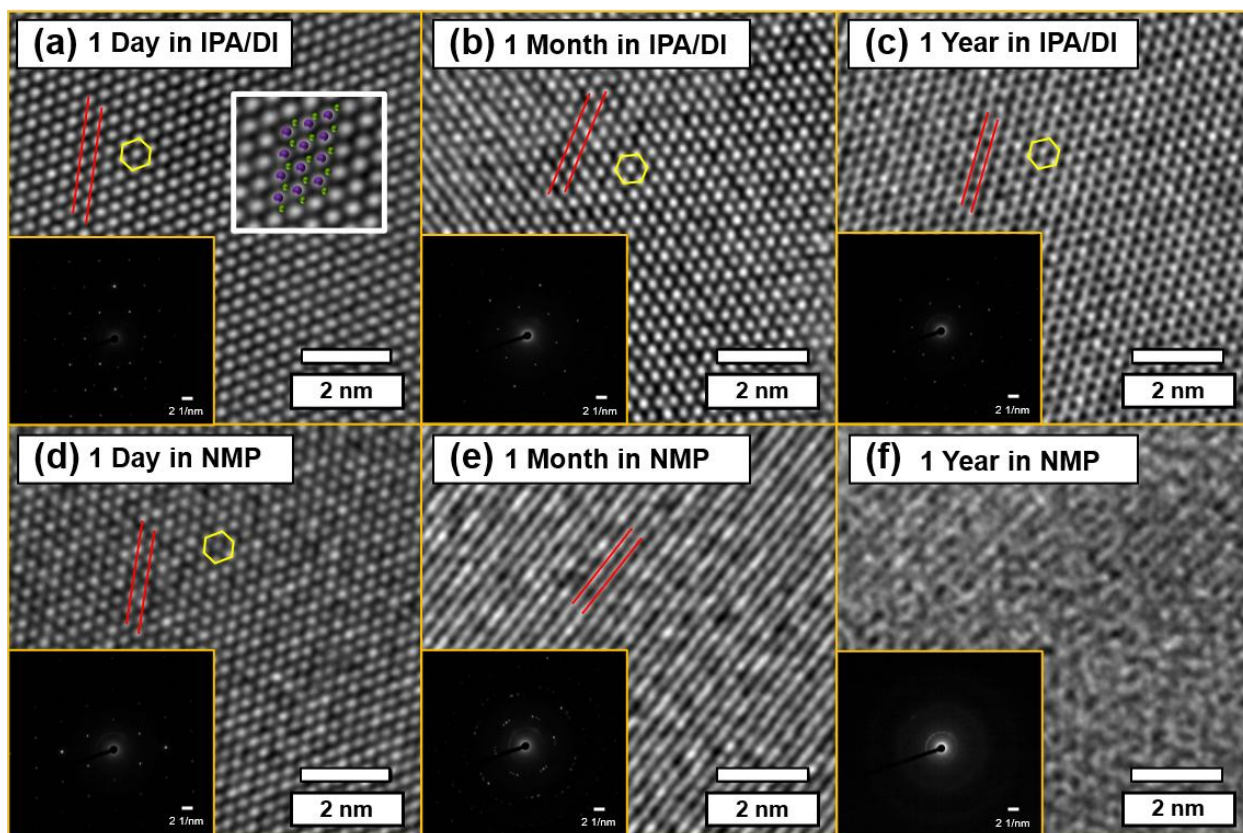


Figure 3. HR-TEM images of WSe₂ nanosheets exfoliated using IPA/DI and NMP, stored for (a) 1 day, (b) 1 month, and (c) 1 year for IPA/DI, and (d) 1 day, (e) 1 month, and (f) 1 year for NMP. The corresponding SAED patterns are shown as insets for each sample.

Based on comprehensive characterisation, WSe₂ nanosheets exfoliated in IPA/DI and NMP and stored for varying durations exhibit distinct local structures, surface compositions, and morphologies. This study also examines how these differences affect their HER performance to identify optimal synthesis and storage conditions. The HER polarisation curves with iR compensation, obtained via linear sweep voltammetry (LSV) in 0.5 M H₂SO₄, are shown in [Figure 4a](#). Among all samples, the WSe₂ nanosheets exfoliated in IPA/DI and stored for one day (black solid line) exhibit the best HER activity, with an overpotential of -0.660 ± 0.002 V vs RHE at -10 mA cm⁻².

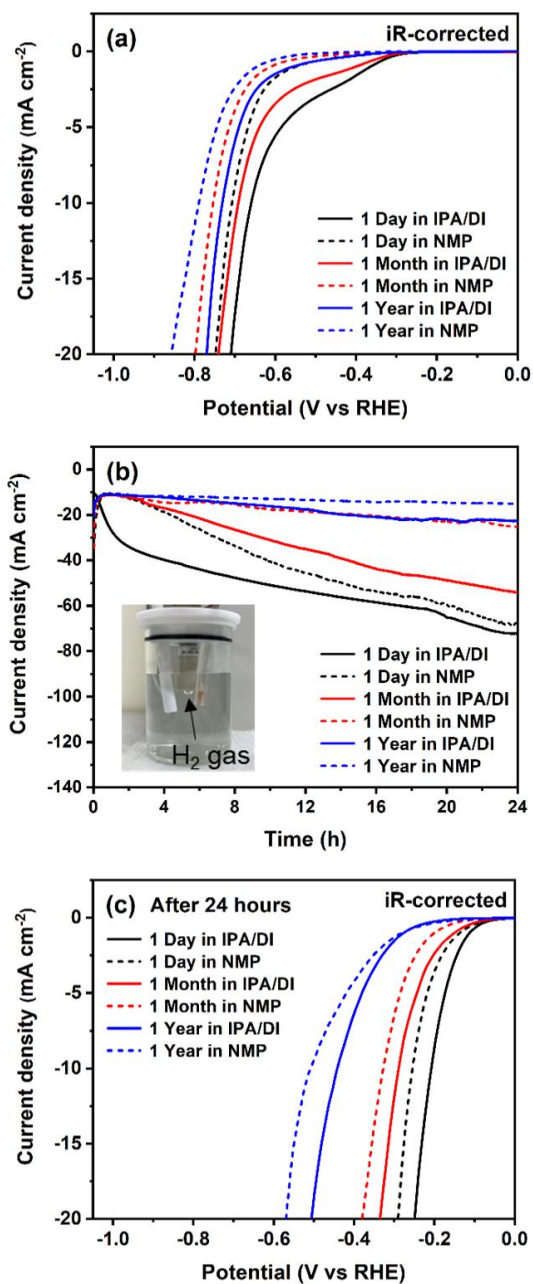


Figure 4. Electrocatalytic performance of as-exfoliated WSe₂ nanosheets in 0.5 M H₂SO₄: (a) *iR*-corrected polarisation curves, (b) chronoamperometry over 24 hours with the setup shown in the inset, and (c) *iR*-corrected polarisation curves post-CA for all samples.

This sample also outperforms others across various electrolytes (KOH and NaCl), as shown in the ESI. The IPA/DI-exfoliated sample stored for one month (red solid line) ranks second (-0.691 ± 0.004 V), surpassing the NMP-exfoliated sample stored for one day (black dotted line), despite having higher oxide content. This might be attributed to the influence of local atomic structure and crystallinity, as revealed by EXAFS, which shows more defined W–Se bonding in the IPA/DI-exfoliated sample. Following in order of performance are: IPA/DI-exfoliated for one year (blue solid line), NMP-exfoliated for one month (red dotted line), and finally, NMP-exfoliated for one year (blue dotted line), which exhibited the poorest HER activity with an overpotential of -0.789 ± 0.005 V vs RHE. Full EIS, iR-compensation, and overpotential data across all conditions and electrolytes are provided in [Figure S5-S7](#) and [Table S4](#).

Long-term stability was assessed via chronoamperometry (CA) over 24 hours in 0.5 M H₂SO₄ at constant potential, with initial current densities of approximately -10 mA cm⁻². As shown in [Figure 4b](#), current density increased significantly over time, reaching around -72 mA cm⁻² for the IPA/DI-exfoliated sample stored for one day, while the NMP-exfoliated sample stored for one year showed only a modest increase to -15 mA cm⁻². Starting potentials and final current densities are summarised in [Table S5](#). Post-CA polarisation curves ([Figure 4c](#)) reveal marked improvements in HER performance. The IPA/DI-exfoliated sample stored for one day exhibited the lowest overpotential after CA (-0.209 ± 0.010 V vs RHE), improving by ~ 0.45 V. In contrast, although the NMP-exfoliated sample stored for one year still showed the weakest performance, its overpotential improved to -0.508 ± 0.007 V vs RHE, a ~ 0.28 V gain. All samples demonstrated enhanced HER activity after CA, likely due to surface activation and increased electrochemical surface area (ECSA), which facilitate the removal of surface impurities and the exposure of additional active sites^{20, 21}. Interestingly, the post-CA polarisation trend differs from the initial

measurements, highlighting the role of oxide content in long-term HER performance. While oxide species can initially contribute to HER via surface oxygen or hydroxyl sites, they tend to degrade under prolonged acidic conditions, diminishing catalytic activity. In contrast, samples with lower oxide content—typically those stored for shorter durations—retain more of the WSe₂ phase and stable Se-edge sites, which are well-established active centres for HER. Moreover, with fewer selenium vacancies, these samples provide more favourable H adsorption (H_{ads}) sites, contributing to superior long-term performance²¹. Detailed overpotential values after 24 hours CA are provided in [Table S5](#) of the ESI.

CONCLUSION

In conclusion, this study highlights the critical influence of solvent choice during LPE and storage duration on the electrocatalytic performance of the exfoliated WSe₂ nanosheets for the HER. A clear time- and solvent-dependent oxidation behaviour was observed, NMP-exfoliated WSe₂ nanosheets exhibiting greater oxidation, less-defined W–Se bonding, increasing selenium vacancies and a more amorphous structure. Additionally, longer storage times led to a significant increase in oxide content. These structural changes impact the HER activity significantly. While IPA/DI-exfoliated nanosheets initially performed best due to their well-preserved structure, after prolonged electrochemical testing, less-oxidised samples exhibited superior performance, emphasising the negative effect of excessive oxidation. All samples showed improved HER activity after 24 hours of chronoamperometry, likely due to surface activation and increased exposure of active sites. The lowest overpotential achieved was -0.206 V vs RHE at -10 mA cm⁻², comparable to platinum. Overall, these findings provide valuable insights and practical guidance

for optimising the synthesis and storage conditions of WSe₂ nanosheets for electrocatalytic applications, particularly in HER.

ASSOCIATED CONTENT

Supporting Information.

Experimental section: XAS and XPS characterisation results analysis. Electrochemical evaluation analysis: EIS analysis and HER performance evaluations in various electrolytes and long-term stability evaluation of WSe₂ nanosheets. The following files are available free of charge.

AUTHOR INFORMATION

Corresponding Author

Pawin Iamprasertkun – *School of Bio-Chemical Engineering and Technology, Sirindhorn International Institute of Technology, Thammasat University, Khlong Luang, Pathum Thani 12120, Thailand; Phone: +66-2-986-9009 ext 2306; Email: pawin@siit.tu.ac.th*

ACKNOWLEDGMENT

This study was supported by Thammasat University Research Unit in Sustainable Electrochemical Intelligent (RU-SEI). The authors acknowledge the Synchrotron facilities from BL1.1W: Multiple X-ray Techniques (XAS), and BL3.2Ua: Photoemission Electron Spectroscopy (PES), Synchrotron Light Research Institute (Public Organization), Thailand.

REFERENCES

1. Fu, Q.; Han, J.; Wang, X.; Xu, P.; Yao, T.; Zhong, J.; Zhong, W.; Liu, S.; Gao, T.; Zhang, Z.; Xu, L.; Song, B., 2D Transition Metal Dichalcogenides: Design, Modulation, and Challenges in Electrocatalysis. *Advanced Materials* **2021**, *33* (6), 1907818.
2. Li, H.; Wu, J.; Yin, Z.; Zhang, H., Preparation and Applications of Mechanically Exfoliated Single-Layer and Multilayer MoS₂ and WSe₂ Nanosheets. *Accounts of Chemical Research* **2014**, *47* (4), 1067-1075.
3. Ross, J. S.; Klement, P.; Jones, A. M.; Ghimire, N. J.; Yan, J.; Mandrus, D. G.; Taniguchi, T.; Watanabe, K.; Kitamura, K.; Yao, W.; Cobden, D. H.; Xu, X., Electrically tunable excitonic light-emitting diodes based on monolayer WSe₂ p-n junctions. *Nature Nanotechnology* **2014**, *9* (4), 268-272.
4. Zhao, W.; Ghorannevis, Z.; Chu, L.; Toh, M.; Kloc, C.; Tan, P.-H.; Eda, G., Evolution of Electronic Structure in Atomically Thin Sheets of WS₂ and WSe₂. *ACS Nano* **2013**, *7* (1), 791-797.
5. Bertolazzi, S.; Brivio, J.; Kis, A., Stretching and Breaking of Ultrathin MoS₂. *ACS Nano* **2011**, *5* (12), 9703-9709.
6. Gholamvand, Z.; McAteer, D.; Backes, C.; McEvoy, N.; Harvey, A.; Berner, N. C.; Hanlon, D.; Bradley, C.; Godwin, I.; Rovetta, A.; Lyons, M. E. G.; Duesberg, G. S.; Coleman, J. N., Comparison of liquid exfoliated transition metal dichalcogenides reveals MoSe₂ to be the most effective hydrogen evolution catalyst. *Nanoscale* **2016**, *8* (10), 5737-5749.
7. Wang, H.; Kong, D.; Johanes, P.; Cha, J. J.; Zheng, G.; Yan, K.; Liu, N.; Cui, Y., MoSe₂ and WSe₂ Nanofilms with Vertically Aligned Molecular Layers on Curved and Rough Surfaces. *Nano Letters* **2013**, *13* (7), 3426-3433.
8. Eng, A. Y. S.; Ambrosi, A.; Sofer, Z.; Šimek, P.; Pumera, M., Electrochemistry of Transition Metal Dichalcogenides: Strong Dependence on the Metal-to-Chalcogen Composition and Exfoliation Method. *ACS Nano* **2014**, *8* (12), 12185-12198.
9. Nicolosi, V.; Chhowalla, M.; Kanatzidis, M. G.; Strano, M. S.; Coleman, J. N., Liquid Exfoliation of Layered Materials. *Science* **2013**, *340* (6139), 1226419.
10. Saisopa, T.; Bunpheng, A.; Wechprasit, T.; Kidkhunthod, P.; Songsiriritthigul, P.; Jiamprasertboon, A.; Bootchanont, A.; Sailuam, W.; Rattanachai, Y.; Nualchimplee, C.; Hirunpinyopas, W.; Iamprasertkun, P., A structural study of size selected WSe₂ nanoflakes prepared via liquid phase exfoliation: X-ray absorption to electrochemical application. *Radiation Physics and Chemistry* **2023**, *206*, 110788.
11. Chavalekvirat, P.; Saisopa, T.; Sornnoi, N.; Hirunpinyopas, W.; Sirisaksoontorn, W.; Busayaporn, W.; Iamprasertkun, P., Tunable properties of WSe₂ nanosheets and nano-dispersion via energy dependent exfoliation. *Materials Reports: Energy* **2025**, 100326.
12. Sierra-Castillo, A.; Haye, E.; Acosta, S.; Bittencourt, C.; Colomer, J. F. Synthesis and Characterization of Highly Crystalline Vertically Aligned WSe₂ Nanosheets *Applied Sciences* [Online], 2020.
13. Song, W.; Zhang, R.; Bai, X.; Jia, Q.; Ji, H., Exposed crystal facets of WO₃ nanosheets by phase control on NO₂-sensing performance. *Journal of Materials Science: Materials in Electronics* **2020**, *31* (1), 610-620.
14. Yamamoto, T.; Teramachi, A.; Orita, A.; Kurimoto, A.; Motoi, T.; Tanaka, T., Generation of Strong Acid Sites on Yttrium-Doped Tetragonal ZrO₂-Supported Tungsten Oxides:

Effects of Dopant Amounts on Acidity, Crystalline Phase, Kinds of Tungsten Species, and Their Dispersion. *The Journal of Physical Chemistry C* **2016**, *120* (35), 19705-19713.

15. Bozheyev, F.; Harbauer, K.; Zahn, C.; Friedrich, D.; Ellmer, K., Highly (001)-textured p-type WSe₂ Thin Films as Efficient Large-Area Photocathodes for Solar Hydrogen Evolution. *Scientific Reports* **2017**, *7* (1), 16003.

16. Jawaid, A.; Nepal, D.; Park, K.; Jespersen, M.; Qualley, A.; Mirau, P.; Drummy, L. F.; Vaia, R. A., Mechanism for Liquid Phase Exfoliation of MoS₂. *Chemistry of Materials* **2016**, *28* (1), 337-348.

17. Lennon, G.; Willox, S.; Ramdas, R.; Funston, S. J.; Klun, M.; Pieh, R.; Fairlie, S.; Dobbin, S.; Cobice, D. F., Assessing the Oxidative Degradation of N-Methylpyrrolidone (NMP) in Microelectronic Fabrication Processes by Using a Multiplatform Analytical Approach. *J Anal Methods Chem* **2020**, *2020*, 8265054.

18. Nualchimplee, C.; Jitapunkul, K.; Deerattrakul, V.; Thaweechai, T.; Sirisaksoontorn, W.; Hirunpinyopas, W.; Iamprasertkun, P., Auto-oxidation of exfoliated MoS₂ in N-methyl-2-pyrrolidone: from 2D nanosheets to 3D nanorods. *New Journal of Chemistry* **2022**, *46* (2), 747-755.

19. Mohsen Asadi, A.; Mohammad Jafari, E., Electron Diffraction. In *Modern Electron Microscopy in Physical and Life Sciences*, Milos, J.; Robert, K., Eds. IntechOpen: Rijeka, 2016; p Ch. 1.

20. Bagheri, R.; Hussain, N.; Wattoo, A. G.; Assefi Pour, R.; Xu, C.; Song, Z., Introducing a self-improving catalyst for hydrogen evolution and efficient catalyst for oxygen evolution reaction. *Journal of Molecular Liquids* **2021**, *334*, 116511.

21. McGlynn, J. C.; Dankwort, T.; Kienle, L.; Bandeira, N. A. G.; Fraser, J. P.; Gibson, E. K.; Cascallana-Matías, I.; Kamarás, K.; Symes, M. D.; Miras, H. N.; Ganin, A. Y., The rapid electrochemical activation of MoTe₂ for the hydrogen evolution reaction. *Nature Communications* **2019**, *10* (1), 4916.

Supporting Information

Table of Contents

| | |
|--|----|
| EXPERIMENTAL PROCEDURES | 17 |
| Liquid-phase exfoliation of WSe ₂ | 17 |
| Material characterisations | 17 |
| Electrochemical measurements..... | 18 |
| CHARACTERISATION RESULTS | 19 |
| X-ray absorption spectroscopy (XAS) analysis | 19 |
| X-ray photoelectron spectroscopy (XPS) analysis..... | 23 |
| ELECTROCATALYTIC PROPERTIES ANALYSIS | 25 |
| Electrochemical impedance spectroscopy (EIS) analysis..... | 25 |
| Evaluation of HER catalytic activity in various electrolytes | 27 |
| Long-term stability evaluation of WSe ₂ nanosheets..... | 30 |
| References | 32 |

EXPERIMENTAL PROCEDURES

Liquid-phase exfoliation of WSe₂

This study investigates the effects of solvent selection and storage duration on the properties of exfoliated WSe₂ nanosheets. To initiate exfoliation, 2.0 g of WSe₂ powder (99.8%, Alfa Aesar) was dispersed in 200 mL of solvent. For the NMP system, the powder was added to 200 mL of N-methyl-2-pyrrolidone (98%, Loba). For the mixed solvent system, WSe₂ powder was added to a 1:1 (v/v) mixture of 100 mL isopropyl alcohol (IPA) and 100 mL deionised water (Milli Q). The resulting suspensions were sonicated in an ultrasonic bath at a power of 271.3 W for 12 hours at 25°C. Following the exfoliation, the dispersions were centrifuged at 5000 rpm for 20 minutes. The exfoliated WSe₂ nanosheets were collected from the supernatant, while the unexfoliated residues remained at the bottom of the tubes. The collected nanosheets were then stored in a cabinet for various durations—1 day, 1 month, and 1 year—to study the effect of storage time. For solid-state characterisation and nanosheets concentration, the exfoliated WSe₂ dispersions were filtered onto PVDF membranes. Omnipore membrane (polyvinylidene fluoride, PVDF, hydrophilic surface, 0.1 µm pore size) was purchased from Merck Millipore Limited. Before filtration, the membranes were pre-weighed using a five-digit precision balance (Mettler Toledo). The dispersions were filtered using a syringe pump at a rate of 20 mL h⁻¹. To prevent further oxidation due to exposure to atmospheric oxygen and moisture, the resulting WSe₂ thin films were stored in a desiccator until further use.

Material characterisations

The thin WSe₂ films deposited on PVDF membranes were utilised for various characterisation techniques requiring solid-state samples. X-ray diffraction (XRD) analysis was performed using a Bruker D8 Advance diffractometer (Bruker AXS GmbH, Germany) equipped with a Cu-K α radiation source ($\lambda = 1.5406 \text{ \AA}$). Scans were conducted over a 2θ range of 10–80°, with a step size of 0.02° and a counting time of 0.2 seconds per step. X-ray absorption near edge structure (XANES) measurements were carried out at Beamline 1 of the Synchrotron Light Research Institute (SLRI), Nakhon Ratchasima, Thailand, to probe the local chemical environment of tungsten. For solid-state measurements, dispersions containing comparable quantities of WSe₂ nanosheets were filtered onto PVDF membranes and measured in transmission mode. For liquid-state analysis, 0.3 mL of exfoliated WSe₂ dispersion was loaded into a polyamide 6 (PA6) liquid cell holder sealed with X-ray transparent Kapton tape. The W L-edge spectra were acquired using photon energy scan points of –150, –20, 60, 100, 200, and 12,000 eV, with corresponding step sizes of 3, 0.3, 1, 3, and 500 eV and dwell times of 2, 2, 3, 5, and 6 seconds, respectively. The total acquisition time per scan was approximately 40 minutes. Due to the low concentration of absorbing atoms in the dispersions, fluorescence detection mode was employed to enhance signal sensitivity. X-ray photoelectron spectroscopy (XPS) was also conducted at SLRI using a SCIENTA R4000 hemispherical analyser at the BL3.2Ua beamline. Surface chemical composition was analysed

using photon energies in the ranges of 40–160 eV and 240–1040 eV. For transmission electron microscopy (TEM), the WSe₂ dispersions were diluted with isopropanol, drop-cast onto carbon-coated copper grids, and dried in a vacuum oven. TEM imaging was performed using a JEOL JEM-2010F microscope operated at an accelerating voltage of 200 kV.

Electrochemical measurements

For electrode preparation, 100 μL of each WSe₂ dispersion ($\sim 1.0 \text{ mg mL}^{-1}$) was mixed thoroughly with 4 μL of Nafion solution (5 wt% in lower aliphatic alcohols and water, Sigma-Aldrich). The resulting mixture was drop-cast onto a polished glassy carbon electrode (surface area = 0.0707 cm^2) and dried in an oven at 55°C for 6 hours. These prepared electrodes were used as the working electrodes for standard electrocatalytic measurements. A three-electrode setup was employed, comprising the WSe₂-coated glassy carbon electrode as the working electrode (WE), a double-junction Ag/AgCl reference electrode (RE), and a polycrystalline platinum wire as the counter electrode (CE), all sourced from PalmSens.

To investigate the electrocatalytic performance under different pH conditions, three types of electrolytes were used. These included an acidic electrolyte of 0.5 M H₂SO₄ with a pH of 0.703, a basic electrolyte of 1.0 M KOH with a pH of 13.43, and a set of neutral electrolytes prepared with varying concentrations of NaCl to simulate seawater conditions. The NaCl concentrations used were 1.0 M, 0.1 M, 0.01 M, and 0.001 M, corresponding to pH values ranging from 6.77 to 5.76. All electrolyte solutions were prepared by dissolving the corresponding materials in Milli-Q deionised water. Prior to all electrochemical tests, the electrolyte solutions were purged with nitrogen gas for 30 minutes to eliminate dissolved oxygen.

For long-term stability testing, 0.5 M H₂SO₄ was chosen as the electrolyte due to the superior HER activity observed in this medium. A rotating disk electrode (RDE) system was employed, using a glassy carbon disk electrode with the same working area of 0.0707 cm^2 (ALS, Japan) as the working electrode. The WSe₂ dispersion mixed with Nafion was drop-cast onto the RDE using the same procedure as for the standard glassy carbon electrode. A carbon rod was used as the counter electrode in place of platinum to prevent potential Pt deposition on the WSe₂ surface, which could artificially enhance HER activity. The Ag/AgCl electrode continued to serve as the reference electrode, supported by prior reports indicating that silver leakage from Ag/AgCl does not contribute to improved HER performance¹.

Linear sweep voltammetry (LSV) was used to assess the HER kinetics, with a scan rate set at 5 mV s^{-1} . All measured potentials were calibrated to the reversible hydrogen electrode (RHE) using the equation: $E(\text{RHE}) = E(\text{Ag/AgCl}) + 0.197 + 0.059 \times \text{pH}$.² To ensure accurate performance analysis, all polarisation curves were corrected for iR drop using 100% solution resistance compensation³. The resistance values used for iR correction were obtained through

electrochemical impedance spectroscopy (EIS) conducted over a frequency range of 0.01 to 10^5 Hz.

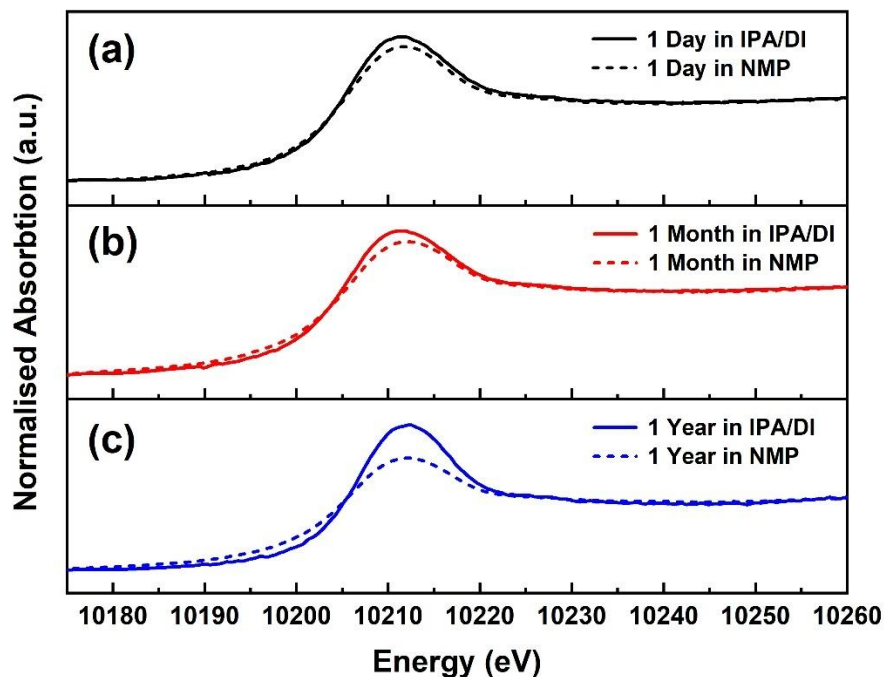
CHARACTERISATION RESULTS

X-ray absorption spectroscopy (XAS) analysis

The normalised W L_3 -edge XANES spectra of all as-exfoliated WSe₂ samples are presented in Fig. S1, with corresponding white line peak positions summarised in Table S1. A noticeable shift in the white line peaks toward higher energies, along with a reduction in peak intensity, was observed for the nanosheets exfoliated in NMP. Additionally, an increase in storage duration led to a further upward shift in peak positions. As shown in Table S1, the white line peaks of WSe₂ nanosheets exfoliated in IPA/DI and stored for one day and one month, as well as those exfoliated in NMP and stored for one day, appear at approximately 10,210 eV—consistent with the W⁴⁺ oxidation state. In contrast, the samples exfoliated in IPA/DI and stored for one year, and those exfoliated in NMP and stored for one month and one year, exhibit peaks shifted to around 10,212 eV, indicative of partial oxidation to W⁶⁺. These values align with the previously published results^{4, 5}. This energy shift reflects a clear time- and solvent-dependent oxidation behaviour, where nanosheets exfoliated in NMP undergo more significant oxidation, which also increases progressively with storage time. The observed reduction in white line intensity suggests possible structural disorder or changes in the local coordination environment associated with higher degrees of oxidation. To further explore these structural variations, an EXAFS analysis was conducted and is discussed in the following section.

Table S1. White line peak positions for all as-exfoliated WSe₂ samples.

| Storage duration | White line peak position | |
|------------------|--------------------------|-------------------|
| | Exfoliated in IPA/DI | Exfoliated in NMP |
| 1 day | 10210.2 eV | 10210.3 eV |
| 1 month | 10210.2 eV | 10211.9 eV |
| 1 year | 10212.2 eV | 10212.3 eV |



FigS. 1 Normalised W L_3 -edge XANES spectra of WSe₂ nanosheets exfoliated in IPA/DI (solid lines) and NMP (dotted lines), after storage durations of (a) 1 day, (b) 1 month, and (c) 1 year.

The Fourier transform (FT) curves derived from the EXAFS spectra of all WSe₂ samples in liquid dispersion form are presented in Fig. S2. For the nanosheets exfoliated in IPA/DI and stored for one day (Fig. S2a) and one month (Fig. S2b), the FT spectra exhibit a dominant W–Se peak located at approximately 2.1 Å, while the first-shell W–O peak appears at around 1.46 Å. Both peaks remain well-defined and consistent in position, indicating minimal structural change over this period. However, after one year of storage (Fig. S2c), a noticeable shift of both peaks to higher radial distances is observed, accompanied by a significant increase in the intensity of W–O peak, which becomes predominant. Despite this, the W–Se peak remains distinguishable. This trend suggests progressive oxidation of the WSe₂ nanosheets over time, leading to the increased formation of W–O bonds. In contrast, nanosheets exfoliated in NMP show a dominant W–O peak even after just one day of storage (Fig. S2d), indicating more immediate and extensive oxidation in this solvent. Although the W–Se peak is still visible at this stage, it becomes increasingly diminished over time. By one month (Fig. S2e) and one year (Fig. S2f), the W–O peak overwhelmingly dominates, and the W–Se peak becomes barely discernible. In addition to changes in peak intensities, a consistent shift of peak positions toward higher radial distances is evident, as detailed in Table S2. This shift, particularly pronounced in the NMP-exfoliated samples and increasing with storage duration, reflects elongation of the W–Se bond. The accompanying decrease in W–Se peak intensity suggests the introduction of selenium vacancies and structural

distortion⁵, contributing to the amorphisation of the nanosheets. These observations confirm the time- and solvent-dependent oxidation behaviour of WSe₂ nanosheets, with NMP promoting more rapid and extensive degradation of the local atomic structure compared to the IPA/DI system.

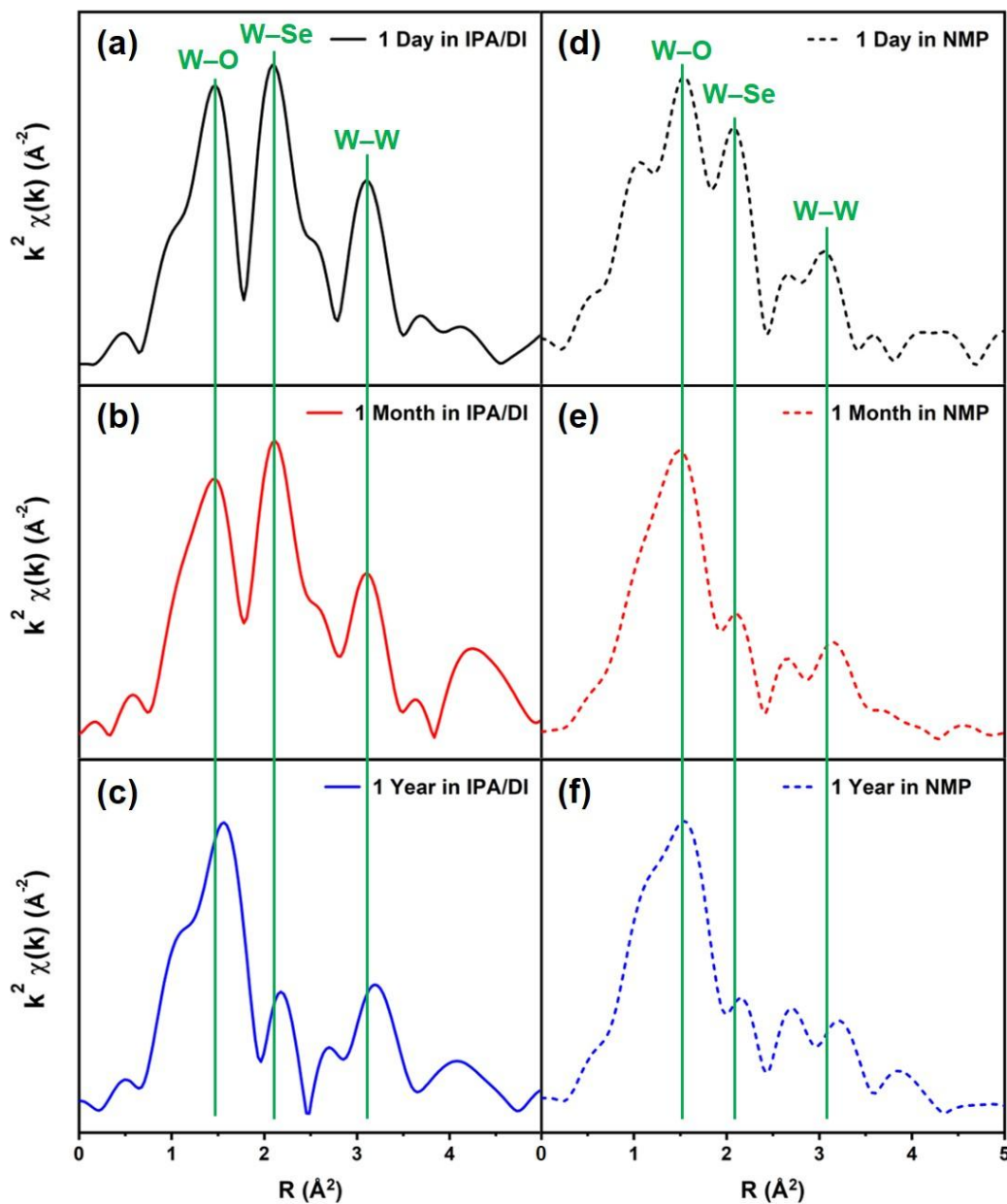


Fig. S2 Fourier-transformed EXAFS spectra showing the radial distribution functions of WSe₂ nanosheets exfoliated in IPA/DI and stored for (a) 1 day, (b) 1 month, and (c) 1 year, and in NMP for (d) 1 day, (e) 1 month, and (f) 1 year.

Table S2. Peak positions derived from the EXAFS spectra of all as-exfoliated WSe₂ samples.

| Storage duration | Radial distances | | | |
|------------------|----------------------|--------|-------------------|--------|
| | Exfoliated in IPA/DI | | Exfoliated in NMP | |
| | W–O | W–Se | W–O | W–Se |
| 1 day | 1.46 Å | 2.08 Å | 1.53 Å | 2.09 Å |
| 1 month | 1.47 Å | 2.11 Å | 1.52 Å | 2.11 Å |
| 1 year | 1.56 Å | 2.18 Å | 1.55 Å | 2.17 Å |

XAS measurements were also conducted on solid-state WSe₂ nanosheets, prepared as thin films by filtering the dispersions onto the PVDF membranes. This was done to enable the comparison between the nanosheets in the solid and dispersion states. In the XANES spectra (Fig. S3a-c), shifts in the white line peak positions and reductions in intensity were observed, particularly for samples exfoliated in NMP across all storage durations. However, these changes were less pronounced than those seen in the dispersion-state measurements. Differences in local atomic structure are more clearly revealed in the EXAFS spectra, shown in Fig. S3d-f. Unlike the dispersion-state spectra, where the first-shell peak corresponds to W–O bond, the solid-state samples—especially those exfoliated in IPA/DI—exhibit a dominant first-shell peak at approximately 2.07 Å, corresponding to the W–Se bond. In samples exfoliated in NMP, this peak shifts slightly to a longer radial distance of around 2.12 Å. Across all samples, the W–Se bond peaks are generally more prominent than the W–O peaks, with the exception of the NMP-exfoliated samples stored for one month (Fig. S3e, dotted red line), where both peaks have comparable intensity, and for one year (Fig. S3f, dotted blue line), where the W–O peak dominates. The distinct W–Se peaks, alongside the broad and faint W–O signals in the solid-state spectra, can be attributed to the re-stacking of nanosheets during the drying process on the PVDF membrane. In contrast, in the dispersion state, the nanosheets remained well-separated and surrounded by the solvent molecules, allowing oxygen atoms to interact more readily with the W atoms and thus producing more pronounced W–O features⁶. Despite these differences, the time- and solvent-dependent oxidation behaviour of the WSe₂ nanosheets remains evident in the solid-state measurements. W–O bond features are more pronounced in the NMP-exfoliated samples, and the W–Se peaks gradually weaken with increased storage time, indicating progressive oxidation and structural degradation.

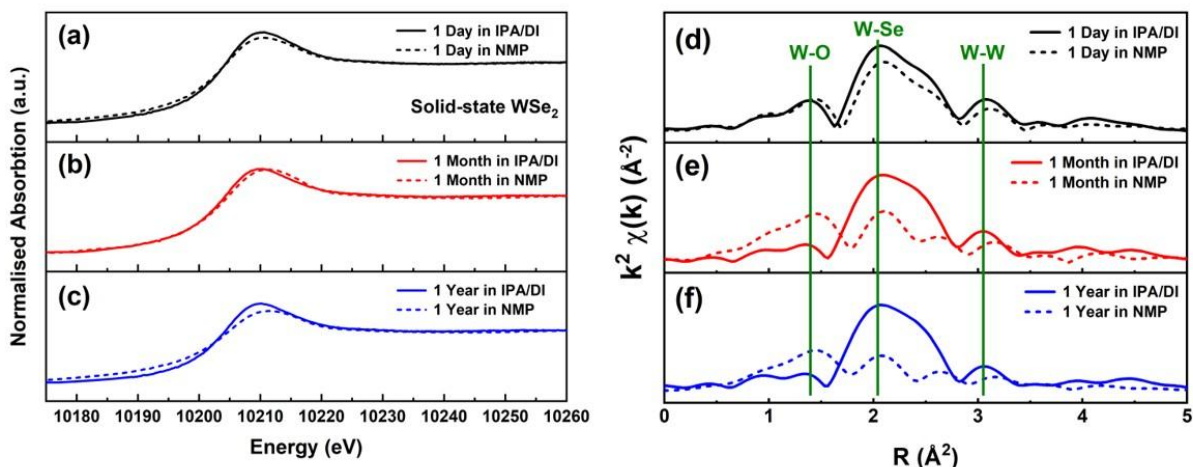


Fig. S3 Solid-state XAS measurements of WSe₂ nanosheets. (a–c) XANES spectra and (d–f) EXAFS spectra of samples exfoliated in IPA/DI and NMP and stored for 1 day, 1 month, and 1 year, respectively.

X-ray photoelectron spectroscopy (XPS) analysis

To analyse the surface chemical composition of the as-exfoliated WSe₂ nanosheets, XPS measurements were conducted. The W 4f spectra of all samples are presented in Fig. S4a. A clear increase in the intensity of the W 4f_{7/2} and W 4f_{5/2} peaks corresponding to WO₃ (W⁶⁺) is observed with increasing storage time, particularly in samples exfoliated in NMP compared to those in IPA/DI. Notably, a shift toward lower binding energies is also evident in samples with higher oxide content. The binding energy values of W 4f spectra for each sample are summarised in Table S3. A similar trend is observed in the Se 3d region, as shown in Fig. S4b. All samples exhibit Se 3d doublet peaks between 53 and 57 eV, corresponding to Se 3d_{5/2} at approximately 54.7 eV and Se 3d_{3/2} at around 55.4 eV. Detailed binding energy values are also listed in Table S3. As discussed in the main text, the decreasing intensity of WSe₂-related peaks and increasing intensity of WO₃-related peaks reflect a time- and solvent-dependent oxidation process. Samples exfoliated in NMP and stored for longer periods exhibit the highest degree of oxidation. In addition to peak intensity changes, the shift in binding energy provides further insight into the oxidation state. Previous studies report binding energies of 32.3 and 34.4 eV for W 4f_{7/2} and W 4f_{5/2} peaks in pristine 2H-WSe₂, respectively. Upon oxidation, these peaks shift to lower binding energies, while new peaks emerge at ~35.6 eV and ~37.7 eV, corresponding to the W 4f doublet of WO₃. This trend aligns with literature findings, indicating that as the oxidation level increases (WO_x, where x ≤ 3), the W 4f and Se 3d binding energies progressively shift downward^{7, 8}. In summary, the XPS results confirm that WSe₂ nanosheets exfoliated in NMP undergo more extensive oxidation, and the degree of oxidation increases with longer storage time, as evidenced by the emergence and intensification of WO₃ peaks and the corresponding binding energy shifts.

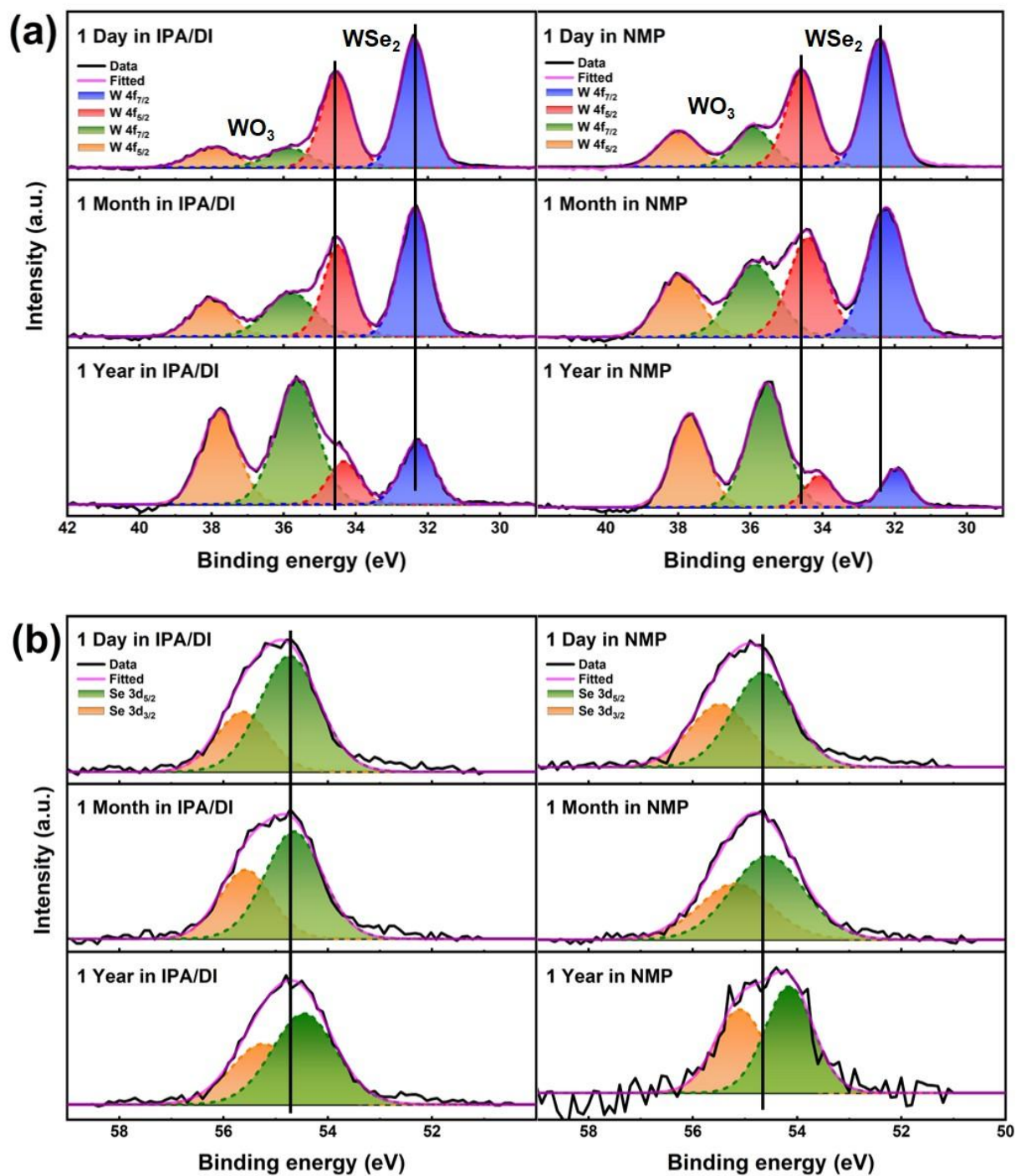


Fig. 4 X-ray photoelectron spectroscopy (XPS) analysis of the as-exfoliated WSe_2 nanosheets: (a) W 4f spectra and (b) Se 3d spectra of all samples.

Table S3. Binding energy values of the W 4f and Se 3d spectra for all as-exfoliated WSe_2 samples.

| | | Binding energies (eV) | | | | | |
|------------------|--------------|-----------------------|---------------------|---------------------|---------------------|----------------------|----------------------|
| Storage duration | Solvent used | WSe ₂ | | WO ₃ | | Se | |
| | | W 4f _{7/2} | W 4f _{5/2} | W 4f _{7/2} | W 4f _{5/2} | Se 3d _{5/2} | Se 3d _{3/2} |
| 1 day | IPA/DI | 32.3 | 34.4 | 35.7 | 37.9 | 54.7 | 55.5 |
| | NMP | 32.3 | 34.4 | 35.7 | 37.9 | 54.6 | 55.4 |
| 1 month | IPA/DI | 32.2 | 34.4 | 35.7 | 37.8 | 54.6 | 55.5 |
| | NMP | 32.2 | 34.3 | 35.7 | 37.8 | 54.5 | 55.1 |
| 1 year | IPA/DI | 32.2 | 34.2 | 35.6 | 37.7 | 54.4 | 55.1 |
| | NMP | 31.9 | 34.0 | 35.4 | 37.5 | 54.1 | 55.0 |

ELECTROCATALYTIC PROPERTIES ANALYSIS

Electrochemical impedance spectroscopy (EIS) analysis

To correct the voltage loss arising from the electrolyte resistance between the working and reference electrodes, iR compensation was applied⁹. EIS was conducted to determine the solution resistance (R_s), which was obtained by fitting the high-frequency region of the Nyquist plot using an equivalent circuit model. In this study, a Randles circuit was employed for the fitting. Fig. S5a displays the Nyquist plot of the WSe₂ nanosheets exfoliated in IPA/DI and stored for one day, shown here as a representative sample. The plot includes both the experimental data and the fitted curve, with the equivalent circuit diagram in the inset. The Nyquist plot exhibits a nearly vertical line, characteristic of capacitive behaviour¹⁰, and notably lacks a semicircle. This absence of the semicircular feature indicates minimal charge storage distribution and strong Ohmic contact between the WSe₂ nanosheets and the substrate^{11, 12}. Similar Nyquist plot profiles were observed for all as-exfoliated WSe₂ samples across all electrolytes tested. This capacitive response is consistent with previously reported Nyquist plots for WSe₂ and WO₃ nanosheets^{10, 13}. Given the lack of a visible semicircle, implying negligible charge transfer resistance (R_{ct}) and fast electron transfer kinetics, 100% iR compensation was deemed appropriate. Under these conditions, the uncompensated resistance (R_u) can reasonably be assumed to represent the solution resistance (R_s) alone³. The R_s values for each sample were extracted from the high-frequency intercept of their respective Nyquist plots. Fig. S5b-g present the R_s values across various electrolytes. No specific trend in the R_s was observed among different WSe₂ samples within the same electrolytes. However, a clear trend was evident across electrolytes: the lowest R_s values, approximately 10 Ω ,

were observed in 0.5 M H₂SO₄ (Fig. S5b) and 1.0 M KOH (Fig. S5c). In contrast, R_s values in NaCl solutions increased significantly with decreasing concentration, with approximate values of 25 Ω, 150 Ω, 1000 Ω, and 5000–10,000 Ω for 1 M, 0.1 M, 0.01 M, and 0.001 M NaCl, respectively. This sharp increase in resistance at lower NaCl concentrations is attributed to the high resistivity of deionised water.

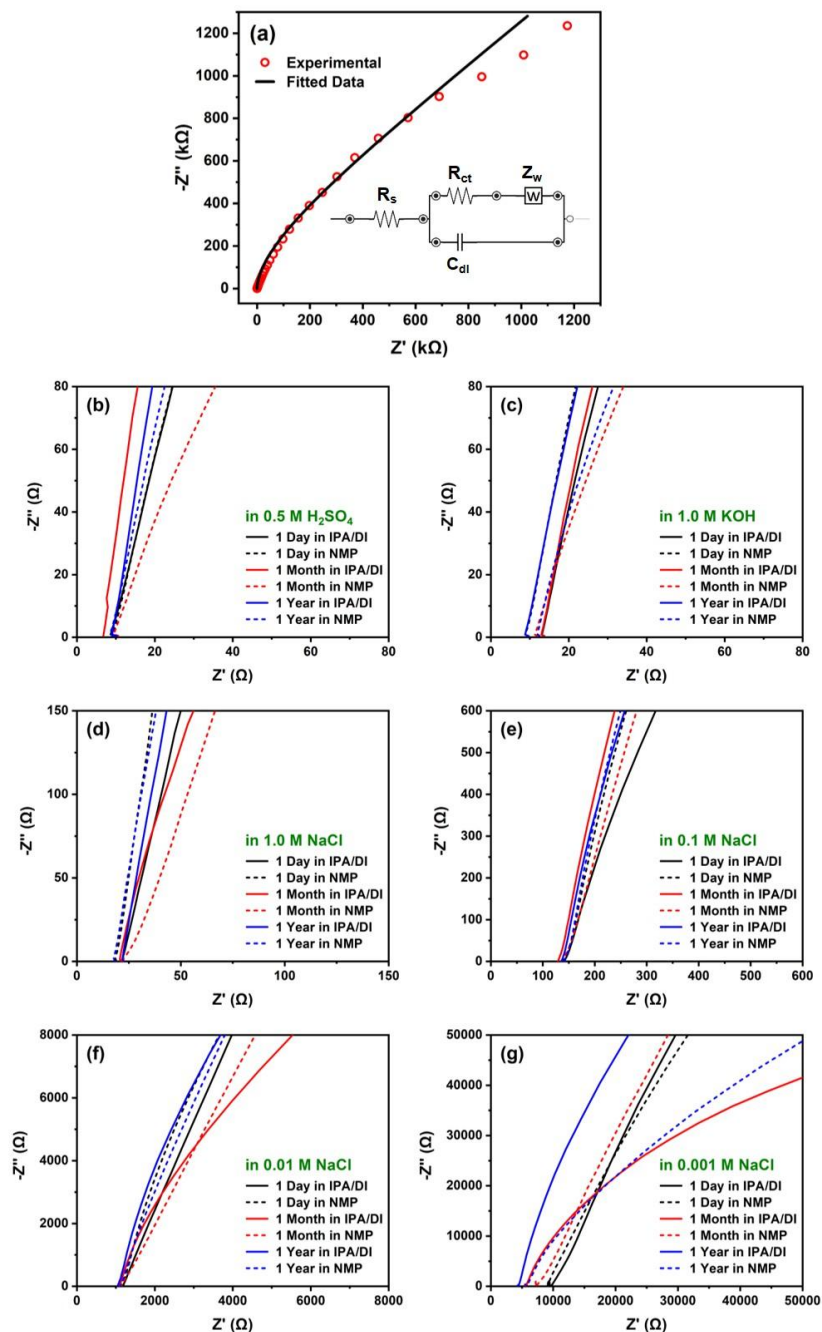


Fig. S5 (a) Representative Nyquist plot of WSe₂ nanosheets exfoliated in IPA/DI and stored for 1 day, showing both experimental data and fitted curve; the inset displays the equivalent circuit used

for fitting. Nyquist plots of all as-exfoliated WSe₂ samples in (b) 0.5 M H₂SO₄, (c) 1 M KOH, (d) 1 M NaCl, (e) 0.1 M NaCl, (f) 0.01 M NaCl, and (g) 0.001 M NaCl.

Evaluation of HER catalytic activity in various electrolytes

To assess the HER catalytic performance of the as-exfoliated WSe₂ nanosheets under different conditions, LSV was conducted in various electrolytes, including 0.5 M H₂SO₄, 1.0 M KOH, and NaCl solutions of varying concentrations. Fig. S6 presents the polarisation curves of all WSe₂ samples in these electrolytes, recorded without iR compensation to evaluate their intrinsic HER activity. Across all electrolytes, the WSe₂ samples followed a consistent performance trend based on their structural integrity and degree of oxidation. Samples with more well-defined W–Se bonds, fewer selenium vacancies, and better crystallinity exhibited superior HER activity. At the benchmark current density of -10 mA cm⁻², the best performance was observed in the sample exfoliated with IPA/DI and stored for 1 day, followed closely by the sample stored for 1 month under the same conditions. The next highest activity was recorded for the NMP-exfoliated sample stored for 1 day. These were followed in descending order by the IPA/DI-exfoliated sample stored for 1 year, then the NMP-exfoliated sample stored for 1 month, and lastly, the NMP-exfoliated sample stored for 1 year, which exhibited the lowest HER activity. This trend remained consistent across all electrolyte systems. The highest electrocatalytic activity was observed in 0.5 M H₂SO₄ (Fig. S6a), with overpotential values at -10 mA cm⁻² summarised in Table S4. While the HER activity in 1.0 M KOH (Fig. S6b) was slightly lower, it remained acceptable. The best-performing sample in KOH, WSe₂ exfoliated in IPA/DI and stored for 1 day, displayed an overpotential of -0.805 ± 0.005 V vs RHE (uncorrected). In NaCl electrolytes, HER performance progressively declined with decreasing salt concentration. At the lowest concentration of 0.001 M NaCl (Fig. S6f), none of the WSe₂ samples reached -10 mA cm⁻², even at potentials as negative as -2.5 V vs RHE. This degradation in performance is attributed to the high resistivity of the diluted NaCl solutions, which limits the current response despite increasing applied voltage. These findings suggest that highly diluted NaCl is unsuitable as an electrolyte for HER applications involving WSe₂ nanosheets.

As previously discussed, 100% iR compensation was applied to all systems. In both 0.5 M H₂SO₄ (Fig. S7a) and 1.0 M KOH (Fig. S7b), the compensation has minimal impact, with only slight reductions in overpotential. Corrected values for 0.5 M H₂SO₄ are presented in Table S4 to compare pre- and post-compensation performance. For NaCl electrolytes at moderate concentrations (1.0 M and 0.1 M; Fig. S7c and S7d), 100% iR correction led to noticeable shifts in polarisation curves toward more favourable potentials. However, in the highly diluted NaCl systems (0.01 M and 0.001 M; Fig. S7e and S7f), full compensation caused significant distortion of the polarisation curves, resulting in a “bend-back” effect and non-physical data. This artifact arises from excessive voltage correction, where the high uncompensated resistance ($R_u > 1000 \Omega$) leads to iR correction values exceeding the practical potential range of the system^{3,9}. For instance, at 10 mA and 1000 Ω , a 10 V correction would be applied. This value is well beyond the electrochemical window of the practical LSV, producing unrealistic current-voltage behaviour. In

such cases, full iR compensation is not viable, and partial correction or no correction should be used instead³. Nevertheless, given the inherently poor HER performance in these highly resistive NaCl electrolytes, their use is not recommended for further WSe₂-based electrocatalytic studies.

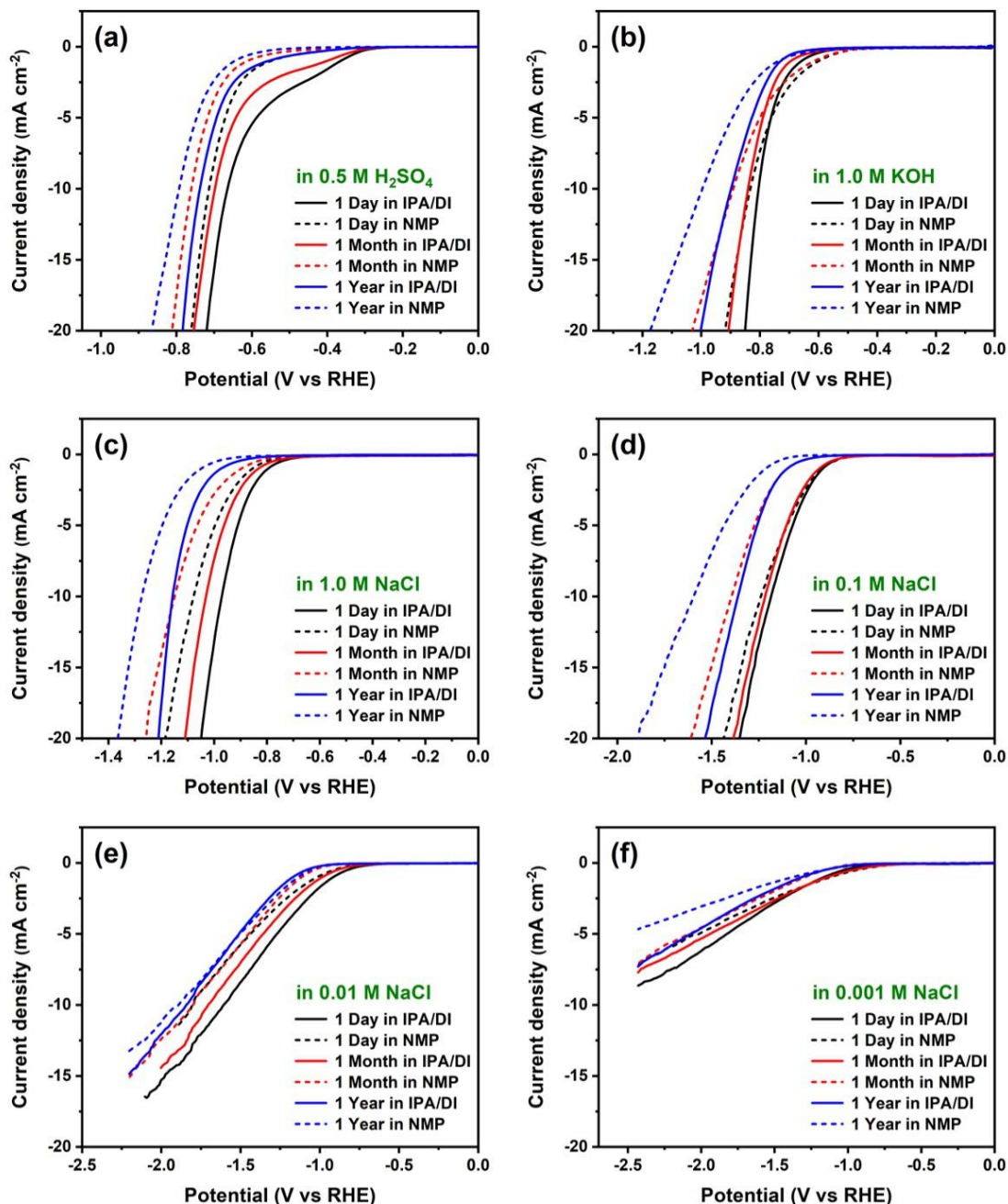


Fig. S6 Polarisation curves without iR compensation for all as-exfoliated WSe₂ samples in (a) 0.5 M H₂SO₄, (b) 1.0 M KOH, (c) 1.0 M NaCl, (d) 0.1 M NaCl, (e) 0.01 M NaCl, and (f) 0.001 M NaCl.

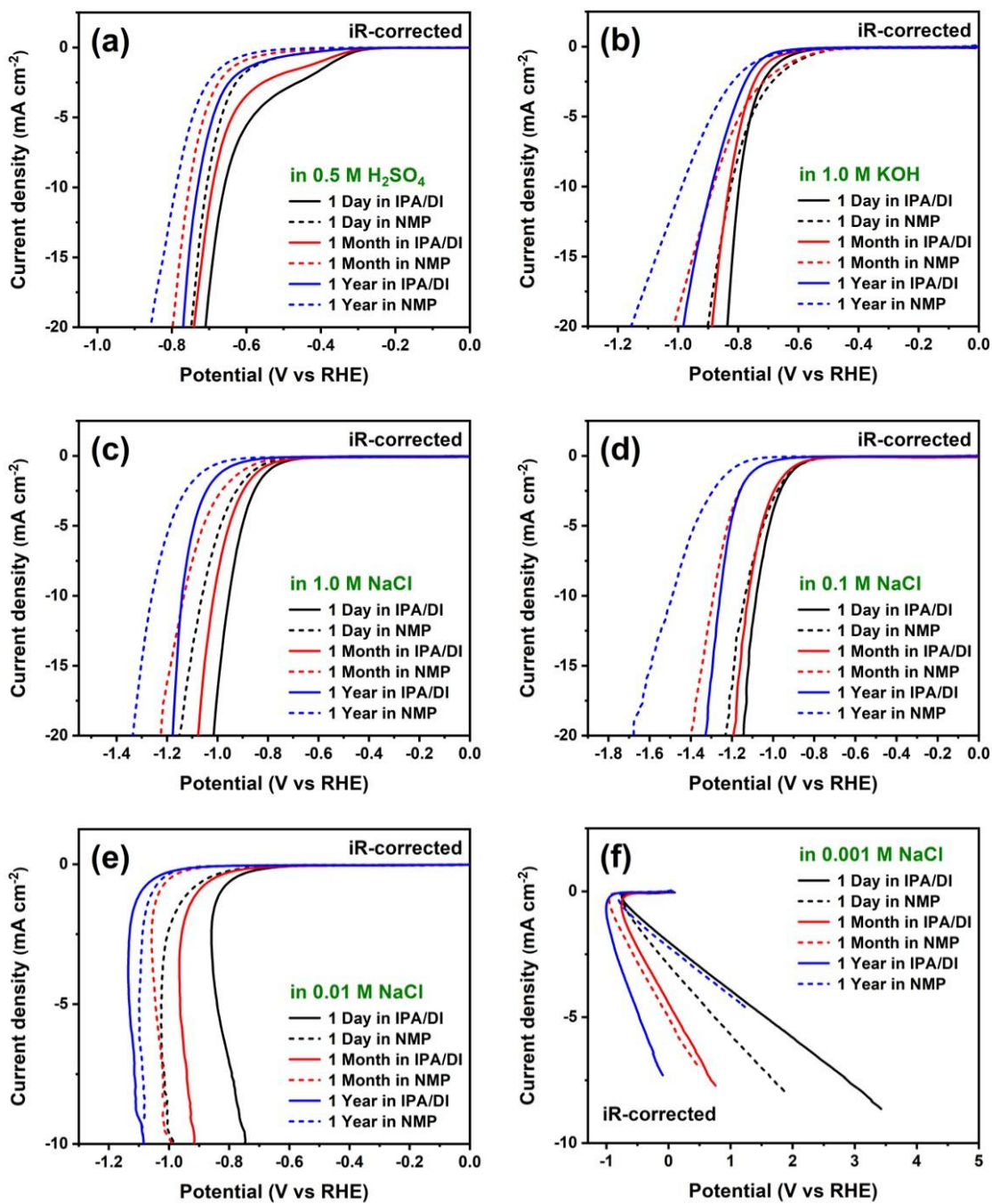


Fig. S7 Polarisation curves with 100% iR compensation for all as-exfoliated WSe₂ samples in (a) 0.5 M H₂SO₄, (b) 1.0 M KOH, (c) 1.0 M NaCl, (d) 0.1 M NaCl, (e) 0.01 M NaCl, and (f) 0.001 M NaCl.

Table S4. Overpotential values at -10 mA cm^{-2} with and without iR compensation in $0.5 \text{ M H}_2\text{SO}_4$ for all as-exfoliated WSe_2 samples.

| Overpotential values (V vs RHE) in $0.5 \text{ M H}_2\text{SO}_4$ at -10 mA cm^{-2} | | | |
|--|-------------------------|---------------------------|-----------------------------|
| Solvent used | Storage duration | No iR compensation | 100% iR compensation |
| IPA/DI | 1 day | -0.665 ± 0.001 | -0.660 ± 0.002 |
| | 1 month | -0.698 ± 0.004 | -0.691 ± 0.004 |
| | 1 year | -0.738 ± 0.010 | -0.731 ± 0.009 |
| NMP | 1 day | -0.714 ± 0.003 | -0.707 ± 0.003 |
| | 1 month | -0.760 ± 0.005 | -0.754 ± 0.004 |
| | 1 year | -0.793 ± 0.005 | -0.789 ± 0.005 |

Long-term stability evaluation of WSe_2 nanosheets.

The long-term stability of the as-prepared electrocatalysts is a critical factor for practical HER applications. Chronoamperometry (CA) measurements were conducted over a 24-hour period at a constant potential, targeting a current density of approximately -10 mA cm^{-2} for each WSe_2 sample. These stability tests were performed exclusively in $0.5 \text{ M H}_2\text{SO}_4$, as this electrolyte demonstrated the highest HER catalytic activity among those tested. As noted previously, all WSe_2 samples exhibited an increase in current density over the 24-hour CA duration, indicating progressive surface activation. [Table S5](#) presents the initial overpotential values and the corresponding final current densities for each sample after a 24-hour test. To assess the electrocatalytic performance following prolonged operation, LSV was also conducted post-CA. The iR-corrected overpotential values at -10 mA cm^{-2} obtained from these LSV measurements are also summarised in [Table S5](#). Among all samples, the WSe_2 nanosheets exfoliated in IPA/DI and stored for one day exhibited the greatest improvement in HER performance, with the reduction in overpotential of approximately 0.45 V (nearly threefold), indicating enhanced catalytic activity. Although the WSe_2 nanosheets exfoliated in NMP and stored for one year continued to show the poorest overall HER performance, they also showed a substantial improvement, with a decrease in overpotential of about 0.28 V . This resulted in a post-CA overpotential of -0.508 V vs RHE, which was still higher than the initial overpotential (-0.660 V) of the IPA/DI-exfoliated sample stored for one day. These improvements across all samples can be attributed to increased

electrochemical active surface area and the removal of surface impurities during prolonged operation. This enhanced exposure of active sites facilitates more efficient electron transfer, thereby contributing to the observed enhancement in HER catalytic activity.

Table S5. Overpotential values at the start and iR-corrected values after 24-hour CA, along with final current densities, for all as-exfoliated WSe₂ samples in 0.5 M H₂SO₄.

| | | Chronoamperometry | | Linear sweep voltammetry | |
|------------------|--------------|----------------------------------|--|--|---|
| Storage duration | Solvent used | Initial overpotential (V vs RHE) | Final current densities (mA cm ⁻²) | Overpotential values pre-CA (V vs RHE) | Overpotential values post-CA (V vs RHE) |
| 1 day | IPA/DI | -0.65 | -72.203 | -0.660 ± 0.002 | -0.209 ± 0.010 |
| | NMP | -0.70 | -66.033 | -0.707 ± 0.003 | -0.254 ± 0.003 |
| 1 month | IPA/DI | -0.70 | -54.087 | -0.691 ± 0.004 | -0.292 ± 0.001 |
| | NMP | -0.75 | -25.284 | -0.754 ± 0.004 | -0.327 ± 0.004 |
| 1 year | IPA/DI | -0.75 | -22.646 | -0.731 ± 0.009 | -0.442 ± 0.008 |
| | NMP | -0.80 | -15.152 | -0.789 ± 0.005 | -0.508 ± 0.007 |

References

1. McGlynn, J. C.; Dankwort, T.; Kienle, L.; Bandeira, N. A. G.; Fraser, J. P.; Gibson, E. K.; Cascallana-Matías, I.; Kamarás, K.; Symes, M. D.; Miras, H. N.; Ganin, A. Y., The rapid electrochemical activation of MoTe₂ for the hydrogen evolution reaction. *Nature Communications* **2019**, *10* (1), 4916.
2. Chowdhury, D. R.; Spiccia, L.; Amritphale, S. S.; Paul, A.; Singh, A., A robust iron oxyhydroxide water oxidation catalyst operating under near neutral and alkaline conditions. *Journal of Materials Chemistry A* **2016**, *4* (10), 3655-3660.
3. Anantharaj, S.; Noda, S., iR drop correction in electrocatalysis: everything one needs to know! *Journal of Materials Chemistry A* **2022**, *10* (17), 9348-9354.
4. Creazzo, F.; Ketkaew, R.; Sivula, K.; Lubner, S., Effects of surface wettability on (001)-WO₃ and (100)-WSe₂: A spin-polarized DFT-MD study. *Applied Surface Science* **2022**, *601*, 154203.
5. Shen, P.; Li, X.; Luo, Y.; Guo, Y.; Zhao, X.; Chu, K., High-Efficiency N₂ Electroreduction Enabled by Se-Vacancy-Rich WSe_{2-x} in Water-in-Salt Electrolytes. *ACS Nano* **2022**, *16* (5), 7915-7925.
6. Chavalekvirat, P.; Saisopa, T.; Sornnoi, N.; Hirunpinyopas, W.; Sirisaksoontorn, W.; Busayaporn, W.; Iamprasertkun, P., Tunable properties of WSe₂ nanosheets and nano-dispersion via energy dependent exfoliation. *Materials Reports: Energy* **2025**, 100326.
7. Yamamoto, M.; Dutta, S.; Aikawa, S.; Nakaharai, S.; Wakabayashi, K.; Fuhrer, M. S.; Ueno, K.; Tsukagoshi, K., Self-Limiting Layer-by-Layer Oxidation of Atomically Thin WSe₂. *Nano Letters* **2015**, *15* (3), 2067-2073.
8. Smyth, C. M.; Addou, R.; McDonnell, S.; Hinkle, C. L.; Wallace, R. M., WSe₂-contact metal interface chemistry and band alignment under high vacuum and ultra high vacuum deposition conditions. *2D Materials* **2017**, *4* (2), 025084.
9. Zheng, W., iR Compensation for Electrocatalysis Studies: Considerations and Recommendations. *ACS Energy Letters* **2023**, *8* (4), 1952-1958.
10. Iamprasertkun, P.; Hirunpinyopas, W.; Deerattrakul, V.; Sawangphruk, M.; Nualchimplee, C., Controlling the flake size of bifunctional 2D WSe₂ nanosheets as flexible binders and supercapacitor materials. *Nanoscale Advances* **2021**, *3* (3), 653-660.
11. Premathilake, D.; Outlaw, R. A.; Parler, S. G.; Butler, S. M.; Miller, J. R., Electric double layer capacitors for ac filtering made from vertically oriented graphene nanosheets on aluminum. *Carbon* **2017**, *111*, 231-237.
12. Bo, Z.; Wen, Z.; Kim, H.; Lu, G.; Yu, K.; Chen, J., One-step fabrication and capacitive behavior of electrochemical double layer capacitor electrodes using vertically-oriented graphene directly grown on metal. *Carbon* **2012**, *50* (12), 4379-4387.
13. Tayebi, M.; Masoumi, Z.; Lee, B.-K., Ultrasonically prepared photocatalyst of W/WO₃ nanoplates with WS₂ nanosheets as 2D material for improving photoelectrochemical water splitting. *Ultrasonics Sonochemistry* **2021**, *70*, 105339.